
Article:
Koçak, M.B., Alver, O., Kaya, B. et al. (2026) Dynamic 1 g model tests on liquefiable sands in newly proposed ETILam soil container and verification through 2D and 3D numerical analyses. Applied Sciences, 16 (9). 4572. ISSN: 2076-3417

https://doi.org/10.3390/app16094572

---

applied sciences

MDPI

Article

Dynamic 1 g Model Tests on Liquefiable Sands in Newly Proposed ETILam Soil Container and Verification Through 2D and 3D Numerical Analyses

M. Batuhan Koçak [1], Ozan Alver [1], Başak Kaya [1,2], Emre Gönülcü [1] and E. Ece Eseller-Bayat [1,*]

[1] Civil Engineering Department, Istanbul Technical University, 34469 Istanbul, Türkiye; kocakm15@itu.edu.tr (M.B.K.); alver16@itu.edu.tr (O.A.); bkaya2@sheffield.ac.uk (B.K.); gonulcu@itu.edu.tr (E.G.)
[2] School of Mechanical, Aerospace and Civil Engineering, University of Sheffield, Sheffield S1 4DT, UK
* Correspondence: ebayat@itu.edu.tr

Abstract

Liquefaction-induced damages related to excess pore water pressure generation in soils and stiffness degradation significantly influence infrastructure and seismic ground response, requiring reliable experimental testing setups and validated numerical models for accurate assessment. This study investigates the free-field liquefaction behavior of saturated sands using the newly proposed ETILam (Enhanced Transparent Impermeable Laminar) soil container under 1 g shaking table conditions. Specimens composed of loose and dense saturated sands overlain by a dry sand layer were prepared and tested under two harmonic motions (0.1 g–2 Hz and 0.2 g–2 Hz), the second motion being two consecutive 6 s excitations. Dynamic response was evaluated through acceleration time histories, shear strains obtained through displacement measurements, excess pore water ratio (r_u), response spectra, transfer functions, and Fourier amplitude computations. Fully coupled effective stress analyses were performed in 2D and 3D using calibrated PM4Sand and P2PSand constitutive models. Experimental results showed limited liquefaction for the lower-amplitude motion, whereas the higher-amplitude motion triggered significant shear strains (up to 10%) and r_u values approaching 0.8, with depth-dependent dissipation patterns between sequential shakings. Numerical simulations reproduced acceleration amplitudes and general pore-pressure trends, with the 2D model providing closer agreement in both generation and dissipation behavior. The findings validate the ETILam container's capability to simulate free-field liquefaction response and demonstrate that a well-calibrated 2D approach can reliably capture the essential features of the observed behavior.

Keywords: shaking table test; laminar box; soil dynamics; liquefaction; numerical modeling

Academic Editor: Roberto Zivieri

Received: 28 February 2026
Revised: 24 March 2026
Accepted: 25 March 2026
Published: 6 May 2026

1. Introduction

The behavior of liquefiable soils during earthquakes results in increases in excess pore water pressures, strain accumulation, and nonlinear stiffness loss in soils, causing significant damage to the infrastructure. Physical model experiments are of great importance for our further understanding of soil liquefaction as well as soil structure interaction in this type of soil. In this context, shaking table (1 g) and centrifuge (n g) tests enable detailed monitoring and measuring of dynamic soil response under controlled cyclic loading conditions. These tests enable the explanation of soil dynamic behavior mechanisms and the development of validated numerical models through advanced instrumentation.

In recent years, centrifuge tests (n g) have been widely used to determine site response and lamination effects in liquefiable soils, to investigate the contribution of drainage to pore water pressure development, and to evaluate the dynamic response and permanent settlement of shallow foundations depending on the degree of liquefaction. Furthermore, re-liquefaction behavior, soil–foundation–structure interaction, and potential improvement/mitigation approaches have been investigated through centrifugal tests [1–9].

Numerous studies in the literature investigate the dynamic response of liquefiable soils, particularly under free-field conditions, using 1 g shaking table tests. A significant part of these studies, using setups such as rigid box (RB) or laminar soil box (LSB/BLSB) to control boundary effects, has evaluated the effects of variables such as peak ground acceleration (PGA), Dr (relative density), r_u/EPWP ratio (excess pore water pressure ratio), shear strain, frequency content, permeability, and lamination (e.g., silt interlayers) on soil amplification or deamplification, response spectrum trends, pore water pressure development, dissipation, and permanent displacement. The findings generally show that liquefaction can cause significant modulus degradation and that, consequently, deamplification of the surface accelerations. The surface response may change more limitedly if partial liquefaction occurs, where drainage/permeability and lamination factors significantly affect r_u development and dissipation. The methods, control parameters, and key findings of the 1 g free-field studies examined in this context are summarized in Table 1 [10–22]. Some of these experimental studies were also validated by numerical analyses.

Table 1. Literature review of 1 g shaking table tests related to this study.

References	Method	Numerical Model	Control Parameters and Variables	Key Findings
Toyota et al. [14]	1 g RB	-	r_u, shaking intensity and freq., slope angle	Shaking intensity ↑ lateral disp ↑ Shaking freq. does not have remarkable influence
Admapira & Derakhshandi [10]	1 g RB + Numerical Study	Dafalias Manzari (OpenSees 2.5.0)	PGA, Sa, Hliq, Zliq, S, EPWP	Liquefaction causes softening and deamplification, amplifying RS for long periods Partial liq. amplifies RS at surface No liq. slightly affects RS at surface Zliq ↑ S ↓, Hliq↑ Sa ↓
Adampira et al. [11]	1 g RB	-	PGA, Dr (%), S, EPWP	Liq ⟶ deamplification, softening, Sa ↓ Partial liq ⟶ slight deamplification, Sa ↑ No liq ⟶ Sa ≅
Ko & Chen [12]	1 g LSB	1-D Shear Beam Approach	r_u, g, acc, G	r_u ↑ ⟶ G ↓ γ ↑ r_u ↑ ⟶ acc↓ at surface
Wang et al. [15]	1 g LSB	-	Dr, r_u, PGA	High PGA and Dr ⟶ dilation High PGA and low Dr ⟶ densification
Basu et al. [13]	Numerical Modeling	PM4Sand (FLAC 2D v 8.0)	r_u, S, k	Calibration of input parameters considering post-shake settlement Effect of permeability on settlement-time histories
Mohsan et al. [20]	1 g LSB	-	Pavement thickness (h_p), width (b_p), S, EPWP	h_p ↑ S ↓ b_p ↑ S ↓
Ecemis [17]	1 g LSB + Numerical Modeling	UBCSand (FLAC 2D v 8.0)	EPWP, volumetric strain (%)	Existence of silt seams affects r_u development, dissipation amount, and duration
Li et al. [21]	1 g LSB	1D Equivalent Analysis	PGA, freq., damping	PGA ↑ ⟶ Freq ↓, D ↑, Amp. ↓
Dou et al. [18]	1 g LSB	-	Acc, PWP, lateral disp.	Existence of Str ⟶ PWP inc. rate ↓ Existence of Str ⟶ depth of liq. ↓ Dissipation rate ↑ Acc. and lat. disp. ↓
Yao et al. [16]	1 g RB	-	r_u, Vane shear resistance (τ_f)	Liquefaction affects intermediate layers more Cost-effective boundary problem solutions
Fan et al. [22]	1 g biLSB	-	PGA, EPWP	Performance of newly designed biLSB (biaxial laminar shear box) with respect to boundary effects was investigated
Mittal & Samanta [19]	1 g LSB	UMAT (ABAQUS v 2022)	PGA, G, EPWP	Input ground motion more amplified under saturated conditions than under dry conditions With increase in PGA, G decreases, while D increases

RB: Rigid box; (B)LSB: (Bilinear) laminar shear box; r_u: excess pore-pressure ratio; Sa: spectral acc., Hliq: liquefiable layer thickness; Zliq: liquefiable layer depth from surface; RS: response spectra; EPWP: excess pore water pressure; G: shear modulus; γ: shear strain; PGA: peak ground acc; S: settlement; D: damping.

In the literature for shaking table tests, rigid or laminar soil boxes have been developed. The main objective in the design of soil boxes is to simulate field behavior in the laboratory. A review of laminar soil boxes used in dynamic soil testing is presented by Bagheri and Eseller-Bayat [23]. Recently, a more enhanced laminar soil container named ETILam (Enhanced Transparent Impermeable Laminar) that better simulates free-field soil conditions under dynamic loading was proposed by Bagheri et al. [24]. Free-field and soil–structure interaction tests were performed in liquefiable soil samples prepared in ETILam. In this paper, free-field liquefaction tests performed in ETILam and enhanced capabilities for simulating the free-field response of liquefiable soil are presented. The performance of ETILam was investigated through sensor measurements and comparison of these measurements with numerical models created in 2D and 3D.

In this study, the newly proposed ETILam soil container and an experimental setup for liquefaction tests are first introduced with details on soil sample preparation and instrumentation. Transfer functions, Fourier amplitude analyses, and response spectra were all obtained and examined in detail based on the experimental measurements, then 2D and 3D numerical models with the most recent soil constitutive models representing liquefaction behavior were generated and compared with the experimental results. Findings of the study shed light on both the experimental and numerical modeling efficiency of liquefaction behavior. This paper presents free-field studies and bases for future soil structure studies in liquefiable soils.

2. Experimental Setup and Specimen Preparation

The experimental study was conducted to investigate the behavior of liquefiable sands under free-field conditions by applying repeatable, controllable seismic loading on a shaking table. In this context, a sand specimen was prepared in the recently designed and manufactured ETILam (Enhanced Transparent Impermeable Laminar) soil container (Bagheri et al. [24]). Various instruments, such as accelerometers, pore water pressure transducers, and LVDTs (Linear Variable Differential Transformers), were positioned at different depths to monitor the soil response during the time history of the motion.

2.1. ETILam Soil Container for Shaking Table Tests

One-dimensional shaking table tests were conducted on saturated sand specimens prepared in an ETILam soil container in the Earthquake Engineering Laboratory at Istanbul Technical University (ITU) to investigate the capability of the newly developed and proposed soil container for the liquefaction testing of sands, as well as to validate 2D and 3D numerical models. The ETILam container was also designed to accommodate future soil–structure interaction (SSI) tests. The experiments were performed using the ARI-1 uniaxial shaking table [25], which has a plan dimension of 2.35 m $\times$ 2.35 m, a horizontal load capacity of 200 kN, a maximum displacement capacity of $\pm$350 mm, and an effective acceleration capacity up to 1 g.

The ETILam soil container, with internal dimensions of 1.60 m $\times$ 1.60 m $\times$ 1.60 m, is composed of 16 plexiglass frames, each measuring 8 cm in height and 4 cm in thickness. These frames are interconnected by a 2 cm flexible sealant material, Sikaflex PRO-3. Vertical support steel roller bearings with a 2 cm diameter were installed on the sidewalls between the laminas, which were attached to an external support frame. The lateral support rollers attached to the external support system keep the container secure, guide each layer in-plane, and prevent torsional effects. To facilitate sample preparation and sensor placement, a steel outer frame system is incorporated with the lamina frames. The ETILam soil container has been awarded a national patent under Patent No. 2022 009917 (Figure 1). The details of the ETILam soil container design can be found in Bagheri et al. [24].

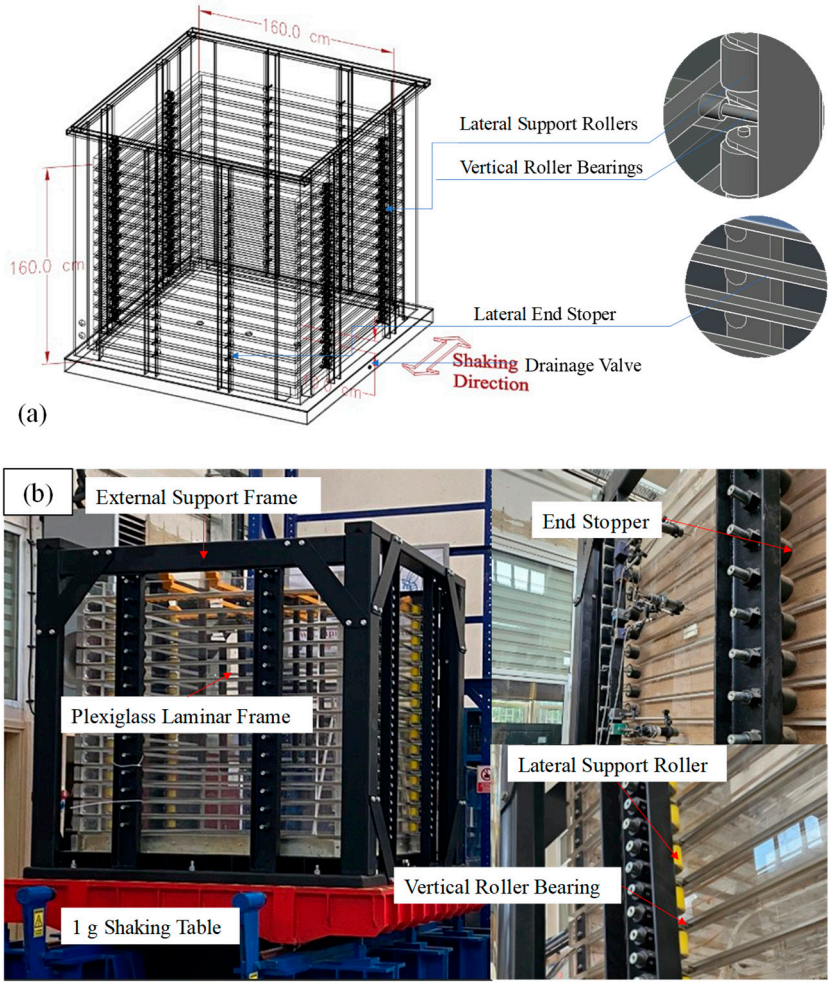

Figure 1. Sketch of Enhanced Transparent Impermeable Laminar (ETILam) soil container (units are in cm) (**a**) and photos of its essential components (**b**).

2.2. Instrumentation

The locations of the accelerometers (ACCs), displacement transducers (LVDTs), and pore water pressure transducers (PPTs) within the soil sample are shown in Figure 2. The accelerometers used were SENSEBOX 7001 (TDG, Ankara, Turkey), with single-axis, low-noise, ±2 g to ±4 g measurement [26]. The pore water pressure transducers were foil strain-gauge piezometers, model 4530, with a range of 0–100 kPa and an accuracy of 0.1 kPa [27]. The displacement transducers were CPD-D LVDT (Linear Variable Differential Transformer)-type sensors from Tokyo Measurement Instruments Laboratory [28].

2.3. Specimen Preparation

The type of sand used in this study was Sile Sand (AFS 40–45), which was also previously utilized in the study conducted by Gurbanov [29]. The sand index parameters and the grain size distribution are presented in Table 2 and Figure 3, respectively. As seen in the gradation curve, the sand type was within the potential soil liquefaction susceptibility gradation limits [30].

A sand sample with a total height of 145 cm was planned, starting from the bottom with 90 cm of saturated dense sand (Dr 90%), followed by 35 cm of liquefiable saturated loose sand (Dr 25–35%), and topped with 20 cm of dry sand. The thicknesses of the soil sample layers were decided for a scale factor (λ) of 20, with the representation of a 7 m liquefiable sand layer and an adequate depth of stiff non-liquefiable zone in real field

conditions. The data regarding the scaling factors used in this study are summarized in Table 3.

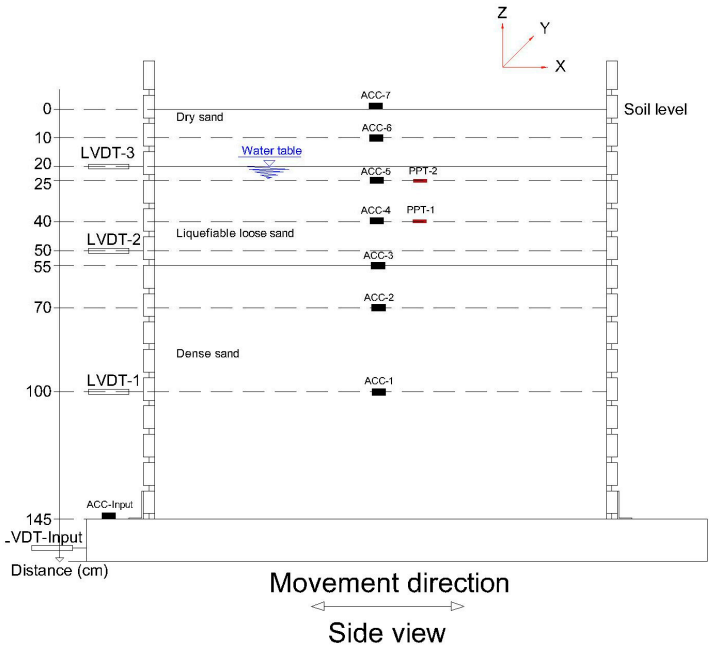

Figure 2. Layout of instruments within the soil specimen.

Table 2. Soil index properties of sand specimen (Gurbanov, [29]).

Soil Index	Test 1	Test 2	Test 3
D_{60}	0.32	0.3	0.28
D_{30}	0.24	0.2	0.19
D_{10}	0.15	0.15	0.15
C_u	2.13	1.8	1.9
C_c	1.15	0.9	0.86
Soil Type	SP	SP	SP
γ_s (g/cm^3)	2.65	2.65	2.65
e_{max}	0.91		
e_{min}	0.57		

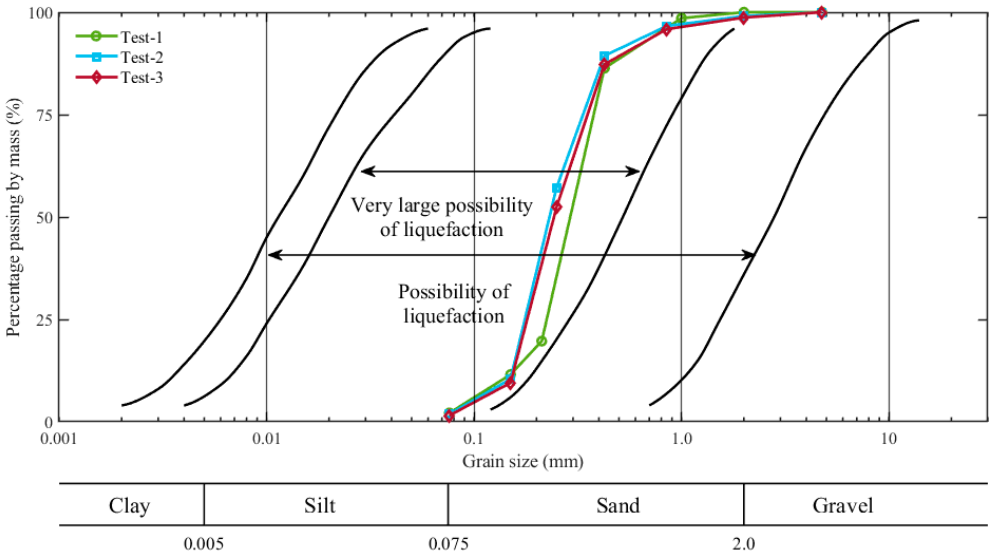

Figure 3. Grain size distribution curve of sand specimen used in the experiments (Gurbanov, [29]).

Table 3. Scaling factors for units.

Parameters	Scaling Factor
Stress	λ
Strain	1
Acceleration	1
Displacement	λ
Frequency	1/λ
Period	λ
Dimension	λ

The required amount of water for the dense sand layer was calculated and transferred into the laminar container using the water column attached to the container's frame (Figure 4). Then, the required amount of sand was added via wet pluviation using different-sized sieves. To achieve the desired density of the 90 cm thick dense sand layer, low-amplitude shaking was applied to the shaking table, and the level of the dense sand was visually checked and measured from the outside. The relative density of the sand can be controlled depending on the sieve diameter and spacing. For the dense sand layer, a sieve with an opening diameter of 0.6 cm and a spacing of 3 × 3 cm was used to achieve maximum density. The loose sand layers were placed into the container through a sieve with a 0.6 cm opening and a 1.5 × 1.5 cm spacing sieve mechanism (Figure 5). The alignment of the instruments placed within the soil was provided using an instrumentation suspension rig specifically manufactured for the container (Figure 5). The accelerometer and pore-pressure transducers were hung on the instrumentation suspension rig before specimen preparation; then, as the instrument became embedded in the soil, the strings were cut. Once all the specimens were ready, the rig was removed before the test. The relative density achieved was ≅90% for the dense layer and ≅30% for the loose layer.

The sand was pumped into steel tanks with capacities of 200 L using a vacuum pump and then weighed (Figure 5). Then, the sand in the tanks was transferred into the laminar container with the help of the lab crane. After the sand specimen was prepared, dynamic motion was applied, and measurements were recorded via various instruments.

For the discharge of the specimen after the test, water was drained through five holes in the bottom of the container and a valve located in the base of the container. A geotextile was placed over the holes to prevent sand from passing through. The specifications of the geotextile were a pore size of O90, 0.100 (±0.020) mm, and a hydraulic permeability (VH50) of 95 (±15) L/(s·m^2).

2.4. Cyclic Shaking Table Tests on Specimens Prepared in ETILam

In this study, a series of shaking table experiments was conducted to investigate the initiation and development of sand liquefaction under controlled seismic loading conditions. Two different displacement time histories were applied to the shaking table. The main objectives of the study were to observe how varying levels of acceleration and duration affect the liquefaction potential of sand, and to verify the efficiency of the newly proposed ETILam soil container.

Two different harmonic displacement records (Figure 6b,d) were applied to the sand specimen prepared in ETILam. The first input motion was characterized by a peak acceleration of 0.1 g at a frequency of 2 Hz, with a duration of 6 s (Figure 6a). The second input motion was stronger, with a peak acceleration of 0.2 g at the same frequency (2 Hz) and a total duration of 12 s, consisting of two consecutive 6 s motions (Figure 6c). Moreover, the second input motion was applied to the shaking table after confirming the dissipation of all excess pore water pressures generated by confirming the hydrostatic water

pressure reading in the sensors. The shaking table tests conducted using the ETILam (Enhanced Transparent Impermeable Laminar) soil container are presented in the supplementary videos (Videos S1–S2), providing a visual overview of the experimental setup and testing procedure.

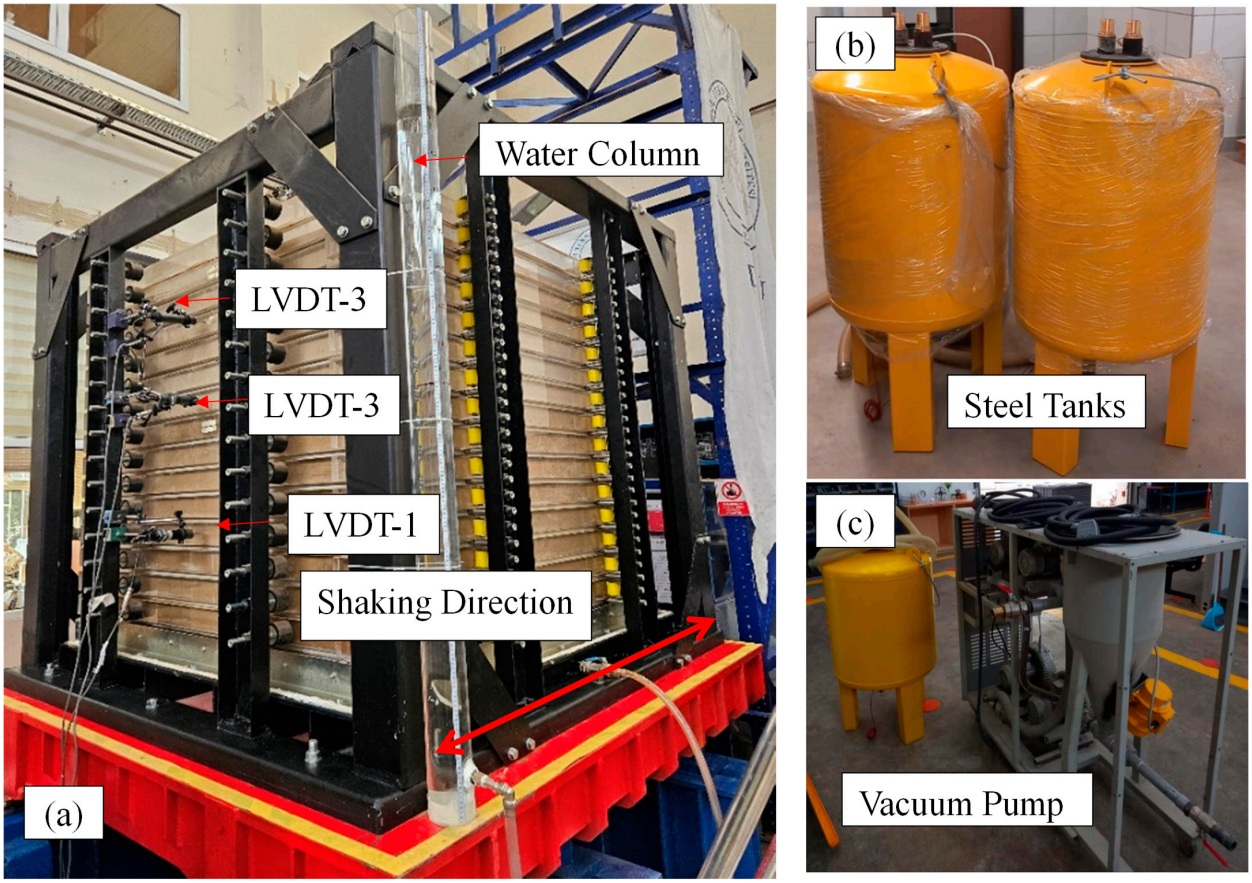

Figure 4. ETILam soil container (**a**), steel tanks (**b**), and vacuum pump (**c**).

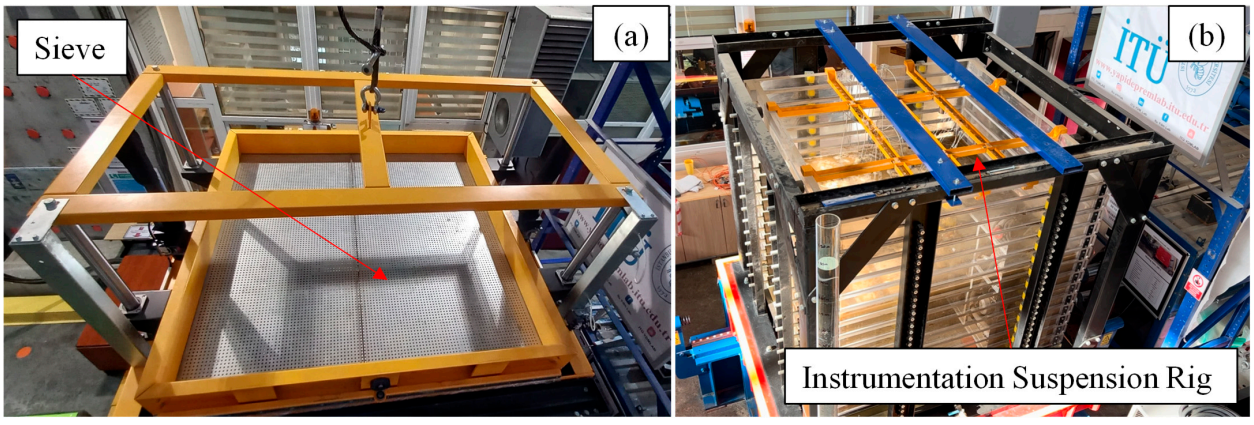

Figure 5. ETILam soil container sieve mechanism (**a**) for specimen preparation and instrument suspension rig (**b**).

During the tests, acceleration measurements were recorded only in Acc4–Acc7. The records of acceleration, displacement, pore water pressure measurements, and data processing results are presented in Section 3. After a sufficient amount of time had elapsed, the settlements were measured, and post-liquefaction relative densities were calculated, as presented in Table 4.

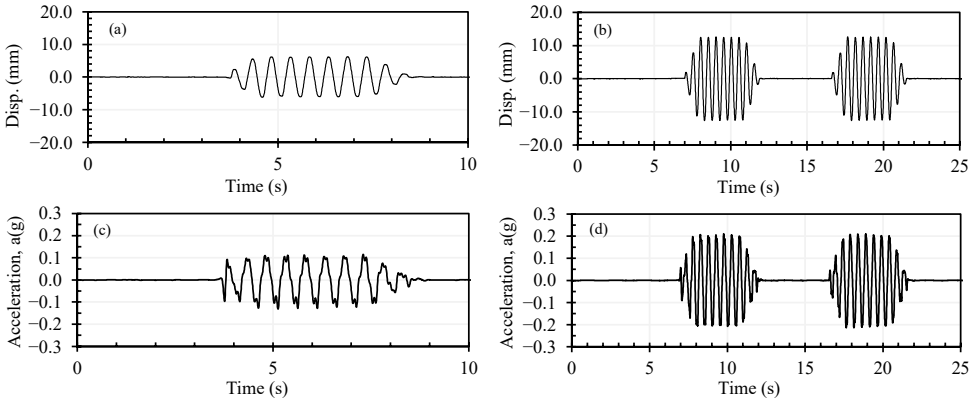

Figure 6. Time histories of the applied input motions: displacement time histories for (**a**) 0.1 g, 2 Hz and (**b**) 0.2 g, 2 Hz; acceleration time histories for (**c**) 0.1 g, 2 Hz and (**d**) 0.2 g, 2 Hz, measured by Acc-Input and LVDT-Input.

Table 4. Settlement and relative density (Dr) values after dynamic loading.

		Initial Dr (%)	Acceleration	Duration	Settlement (cm)	Final Dr (%)
Experiment 1	Loose Sand layer Dense Sand layer	30.0 90	0.1 g	6 s, 1 excitation	1–1.5 0	35–40 90
Experiment 2	Loose Sand layer Dense Sand layer	35–40 90	0.2 g	6 s, 2 excitations	3.5–4 0.5	60–65 ≅90

For the discharge of the sand specimen, the drainage of water was provided through the bottom. Since the sample was still moist, it was challenging to use the vacuum pump at this stage. In order to dry the moist sand, electrodes were embedded in the sample. The electrodes were inserted approximately 30–40 cm deep, and after waiting for 1–2 h, the dried portion was vacuumed. This process was repeated until the entire box was emptied, as shown in Figure 7.

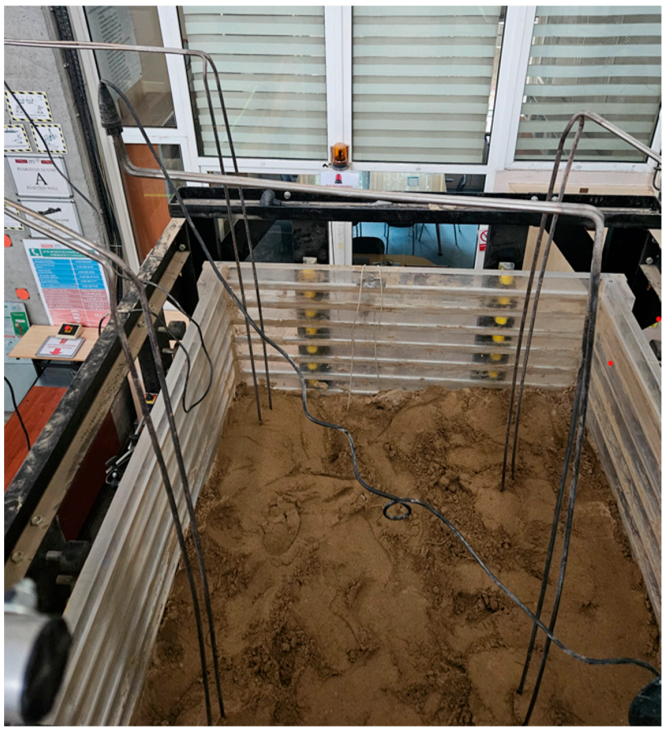

Figure 7. The drying process of the sand sample through electric rods before removal.

3. Numerical Analyses of Cyclic Shaking Table Tests

This section presents details of our numerical studies, beginning with laboratory experiments that represent the dynamic behavior of the sand sample used in the shaking table tests. Accordingly, CDSS (Cyclic Direct Simple Shear) tests on the same material under different cyclic stress ratios (CSRs) were conducted and modeled to reveal the sample's stress–strain characteristics and liquefaction tendency under cyclic loading.

The following subsection presents the 2D and 3D numerical modeling and details of shaking table test simulations. Fully coupled numerical analyses of effective stress-based time-history simulations were performed using the finite difference (FD) method in FLAC2D 8.1 [31] and FLAC3D 7.0 [32]. The analyses utilized the PM4Sand (Version 3.2) (in FLAC2D) and P2PSand (in FLAC3D) constitutive models to capture the dynamic response of liquefiable sands subjected to seismic loading. A series of calibration analyses was performed to simulate the dynamic behavior of Sile Sand (AFS 40–45). In the two-dimensional calibration analyses, the PM4Sand model (Ziotopoulou & Boulanger [33]), a stress-ratio-controlled, critical-state-compatible, bounding-surface plasticity model, was employed to represent the dynamic behavior of Sile Sand. This model was developed based on the DM04 model (Dafalias & Manzari [34]), which is used in geotechnical earthquake engineering applications. In 3D analyses, the P2PSand [35] model was used, which is a stress-based constitutive model designed to capture the behavior of sandy soils under cyclic loading conditions. The model accounts for essential mechanisms, including stiffness degradation, contractive/dilative tendencies, and the resulting accumulation of excess pore water pressure during cyclic shearing. The cyclic shaking table tests were conducted with a Rayleigh damping ratio of 0.005. Numerical analyses were performed for both the two- and three-dimensional cases. In addition, the flow-on option was used during both the dynamic loading and the post-shaking reconsolidation phase. A lateral earth pressure coefficient at rest of $K_0 = 0.5$ was adopted in both models to define the initial stress state.

3.1. Calibration Analysis

The calibration analyses were first carried out to determine the constitutive model input parameters, and the resulting PM4Sand (FLAC2D) and P2PSand (FLAC3D) numerical calibrations were subsequently adopted in the shaking table simulations to represent the seismic response of the liquefiable sands.

The calibration analyses were performed using results from CDSS (Cyclic Direct Simple Shear) tests performed at the Istanbul Technical University (ITU) Soil Dynamics Laboratory. These CDSS tests were conducted on specimens prepared with varying relative densities as part of the thesis studies by Deniz [36] and Gurbanov [29]. The tests were stress-controlled and performed for different CSR (cyclic stress ratio) values. CSR-N_{cycle} (number of cycles) curves obtained from dynamic DSS experiments were used to validate the numerical model input parameters. In these curves, the N_{cycle} values represent the cycle number at which the r_u value reaches 1, i.e., the excess pore water pressure is approximately equal to the initial effective stress.

Only the primary input parameters were used in the two-dimensional calibration analyses conducted using the PM4Sand model. These parameters included the relative density (D_r), the small-strain shear modulus value (G_0) that governs the initial shear modulus (G_{max}), and the contraction rate parameter (h_{p0}).

Dafalias and Manzari [34] included the dependence of G on the void ratio. However, Ziotopoulou and Boulanger [33] did not include this approach and suggested a G_0 calcula-

tion based solely on one constant: V_s, the shear wave velocity. The following equation was used to determine the G_0 value for the PM4Sand model:

$$G_0 = \frac{\rho V_s^2}{p_a}\left(\frac{p_a}{p}\right)^{1/2} \quad (1)$$

where V_s is shear wave velocity (m/s), p_a is atmospheric pressure (101.3 kPa), ρ is mass density (kg/m^3), and p is mean effective stress (kPa).

The secondary input values of the PM4Sand constitutive model were accepted as default, and the contraction rate parameter (h_{p0}) values were determined as 0.50, 0.42, and 0.45 for Dr 30%, Dr 40%, and Dr 50%, respectively. The dense sand material (Dr 90%), on which laboratory tests were not performed to calculate the CRR-N_{cycle} curve, was also calibrated based on the 50% probability of liquefaction (PL) CRR curve at 15 cycles from the Boulanger & Idriss [37] liquefaction triggering procedure.

The input parameters in the P2PSand model (for 3D analyses) were internally calibrated based on the relative density. However, plastic modulus parameter (ho) and cyclic resistance factor (Kc) values were modified to capture the soil response obtained from the CDSS results. The CSR-N_{cycle} curve comparisons for the condition of liquefaction, where the excess pore water pressure ratio equals 1, are presented in Figure 8, based on both experimental and 2D–3D numerical analyses. The input parameters related to test-1 and test-2 are presented in Tables 5 and 6, respectively. Permeability values were entered identically for both 2D and 3D numerical analyses. For 3D analyses, a relative density value of 85% was entered due to the upper limit of the related constitutive model.

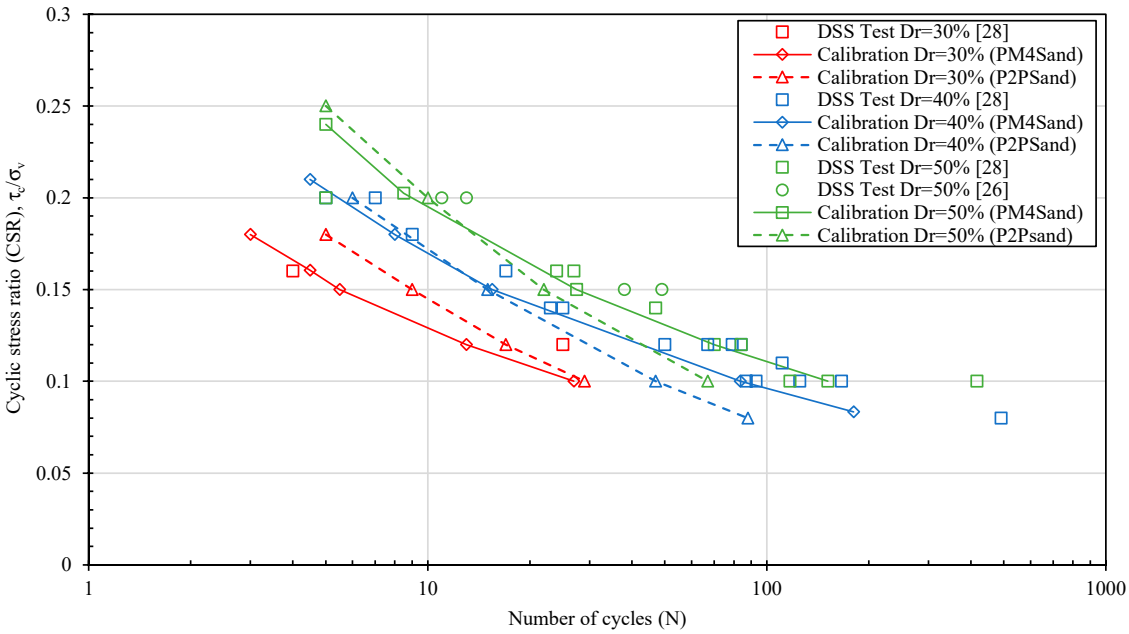

Figure 8. Cyclic stress ratio versus the number of cycles. Comparisons for Dr at 30%, 40%, and 50% [29,36].

Table 5. Two-dimensional numerical analyses of PM4Sand input parameters.

Soil	D_r (%)	G_0	h_{p0}	e_{min}	e_{max}	ϕ_{cv}	k (m/s)
Loose Sand [1]	30	410	0.5	0.57	0.89	33°	1.0×10^{-4}
Loose Sand [2]	35	450	0.42	0.57	0.89	33°	1.0×10^{-4}
Dense Sand	90	1050	2	0.57	0.89	33°	1.0×10^{-4}

[1] Used for the first motion; [2] used for the second motion.

Table 6. Three-dimensional numerical analyses of P2PSand input parameters.

Soil	D_r (%)	G_r	h_0	K_c
Loose Sand [1]	30	384	0.5	0.15
Loose Sand [2]	35	446	0.5	0.15
Dense Sand	85	1066	1.7	0.007

[1] Used for the first motion; [2] used for second motion.

3.2. Numerical Modeling of Shaking Table Tests of Specimens Prepared in ETILam

The 2D and 3D models were generated and are presented in Figure 9, where the geometry, boundary conditions, and soil layering of the sand specimen in ETILam are presented. The two-dimensional numerical analyses were performed based on plane strain conditions, and the geometry of ETILam was modeled as the cross-section perpendicular to the shaking direction. While the vertical boundary conditions in the static phases were fixed horizontally and free vertically, fixity was provided in both directions at the bottom boundary; static stress calculations were performed. In dynamic analyses, the vertical boundaries of the model are defined by attached boundary conditions, in which vertical deformations are limited while horizontal deformations are allowed, consistent with the ETILam experimental setup boundary conditions. The acceleration–time input was defined at the bottom boundary of the numerical model, which was vertically fixed. A numerical model that was more sensitive and compatible with the shaking table with attached vertical boundary conditions is a future aim. A numerical model that was more sensitive and compatible with the ETILam soil container on the shaking table was aimed to be developed with the introduced attached vertical boundary conditions in the model.

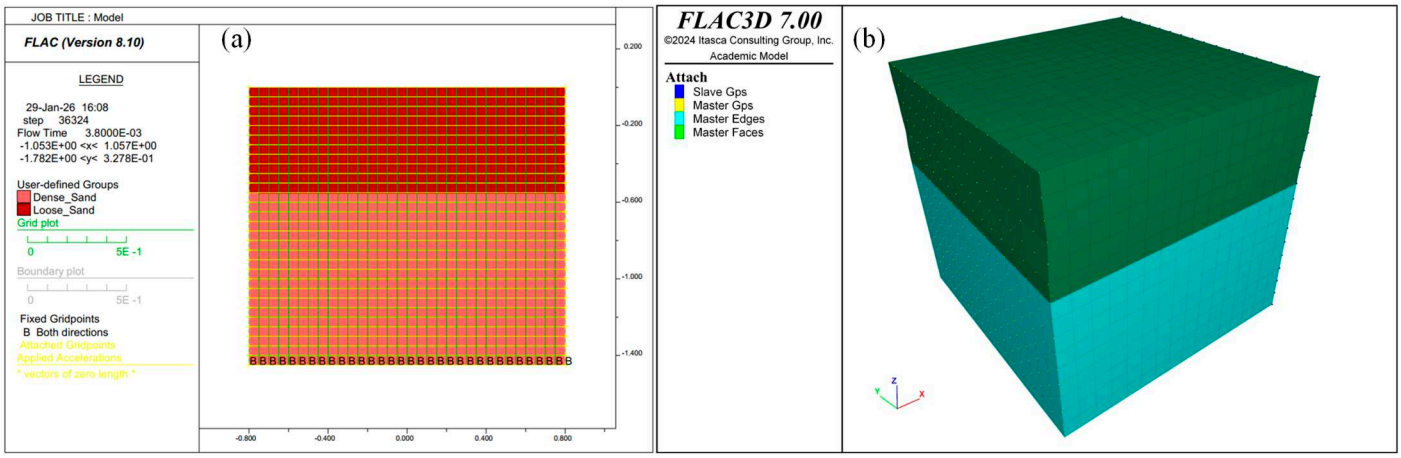

Figure 9. (**a**) 2D numerical model; (**b**) 3D numerical model.

In the 3D model, vertical boundaries are fixed during the static equilibrium stage, while they are attached to allow tied boundary conditions during the dynamic shaking stage of the analysis. The shaking table test numerical analyses for both the two- and three-dimensional cases were performed using calibrated soil models. The test analyses were performed separately for the first and second motions, taking into account the densification due to the first shaking.

3.3. Comparative Results and Findings of Experimental Tests and Numerical Analyses

The sensor measurements from shaking table tests and corresponding numerical analysis results are compared in this section to assess the 2D and 3D models' capability of capturing the experimental dynamic response of the liquefiable sand, as well as to validate the performance of the newly proposed ETILam soil container. The discussion focuses on

the level of agreement and observed deviations in the excess pore water pressure responses and acceleration time histories.

The response spectra for each test were calculated using the acceleration time histories obtained from accelerometers at various depths, as detailed in Section 2.2. The recorded acceleration time histories were processed by applying a bandpass filter (0.5–8 Hz) and performing baseline correction to remove noise and long-term drift.

The response spectra were then determined using the Newmark Integration method, with a damping ratio of 0.05 (Figure 10). These analyses aimed to identify the system's dominant frequencies and evaluate the effects of liquefaction on the dynamic response. All the analyses were performed for Accs-4–7, since Acc-1–Acc-3 malfunctioned due to water leakage into the sensors during the tests. The spectral acceleration at each sensor level shows the amplification at the input motion frequency (2 Hz), and the fundamental frequency of the soil stratum (5–6 Hz), as shown in Figure 10. Similar findings were also observed in the Fourier amplitude spectrum results (Figure 11).

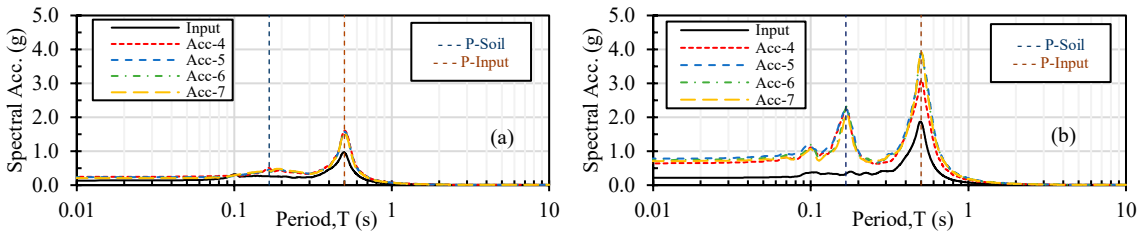

Figure 10. Response spectra: (**a**) 0.1 g, 2 Hz, (**b**) 0.2 g, 2 Hz.

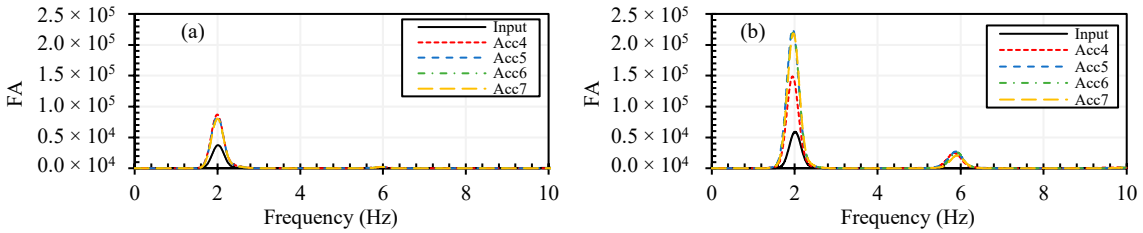

Figure 11. Fourier amplitudes: (**a**) 0.1 g, 2 Hz, (**b**) 0.2 g, 2 Hz.

Subsequently, the Fourier amplitudes were normalized with respect to the base motion to compute amplification ratios. The amplification ratios represent the relative increase in amplitude at different depths compared to the input motion. This approach helped identify the frequency ranges where significant amplification occurred due to soil response, thereby indicating the fundamental period of the soil column. The results for each motion are presented separately in Figure 12 and show that the maximum amplification again corresponds to the fundamental frequency of the sand, 6 Hz.

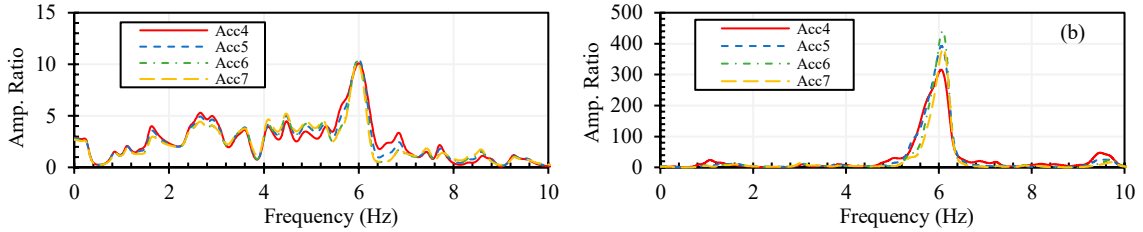

Figure 12. Amplification ratios: (**a**) 0.1 g, 2 Hz, (**b**) 0.2 g, 2 Hz.

The measurements from LVDT instruments were compared with displacement time histories computed from acceleration measurements, confirming that the displacements of

the sand in the center were in line with the displacement of the plexiglass lamina at the same level, as shown in Figure 13. Also, the comparisons verified that the accelerometers did not change their alignment. This comparison also led us to decide on the tied degree boundary conditions of the numerical models.

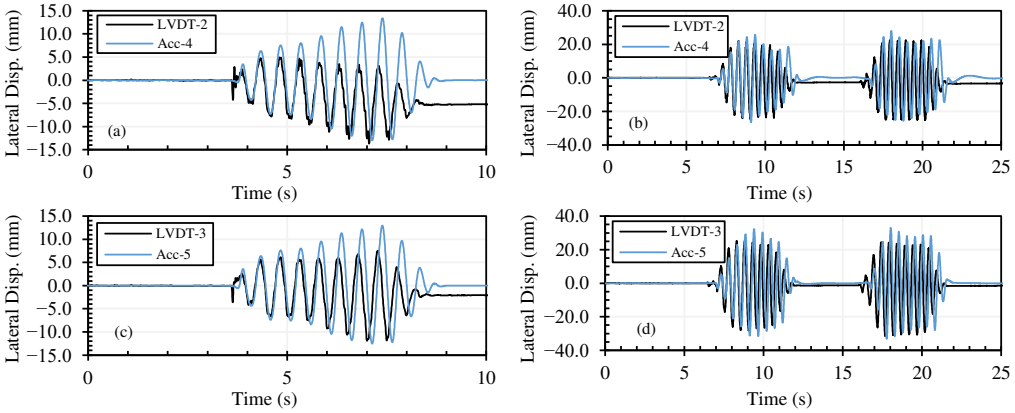

Figure 13. Comparison of lateral displacement measured in LVDTs and computed from accelerometer measurements: (**a**,**c**) for 0.1 g input motion; (**b**,**d**) for 0.2 g input motion.

The absolute shear strain values were calculated by considering the relative differences and heights between the lateral displacements measured by the LVDTs. Figures 14 and 15 present the r_u generations together with acceleration and strain time histories at the two PPT levels. Although strain levels for the first motion were between 0.2 and 0.5%, that is sufficient to trigger liquefaction (Figure 14c,d). r_u generations at PPT-1 and PPT-2 were recorded as around 0.6 and 0.2, respectively (Figure 14e,f). During the second motion, the shear strain amplitude reached 10% at PPT-1 and 5% at PPT-2 levels (Figure 15c,d), generating a maximum $r_u = 0.8$ (Figure 15e,f). The effect of subsequent motions was also observed during the second test. Excess pore water pressures at the deeper PPT were not dissipated, whereas excess pore water pressure at the lower PPT started to dissipate between the two motions and regenerated during the subsequent second part of the motion.

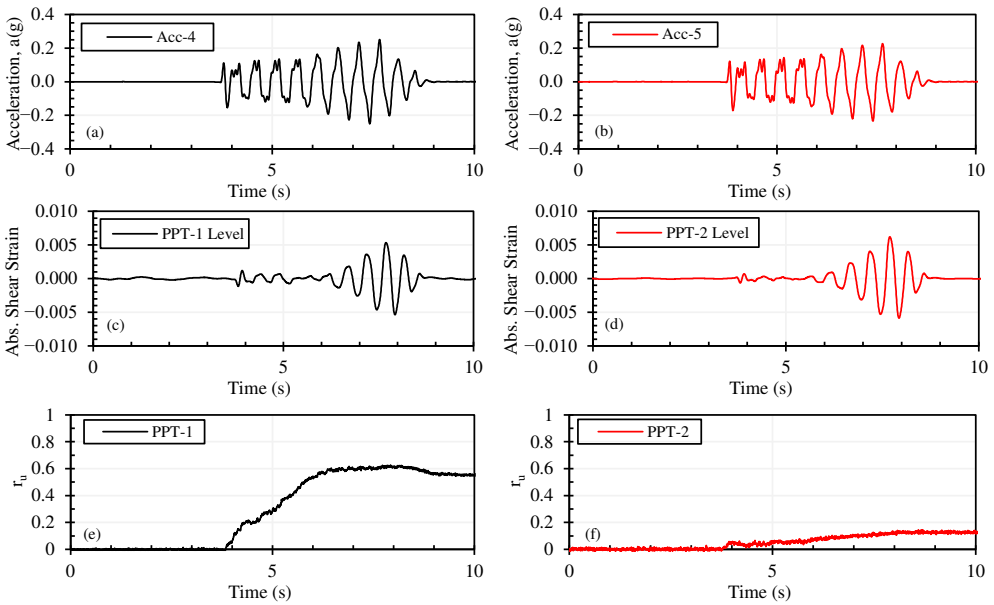

Figure 14. Acceleration time histories (**a**,**b**), computed absolute shear strain time histories (**c**,**d**) from accelerometer measurements, and r_u time histories (**e**,**f**) at PPT-1 and PPT-2 elevations, respectively, for the first motion.

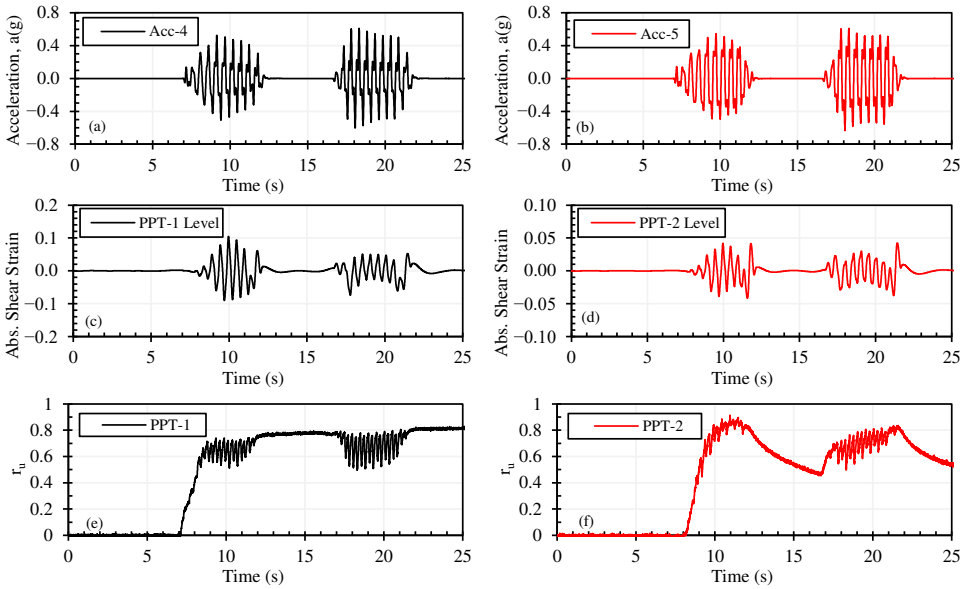

Figure 15. Acceleration time histories (**a**,**b**), computed absolute shear strain time histories (**c**,**d**) from accelerometer measurements, and r_u time histories (**e**,**f**) at PPT-1 and PPT-2 elevations, respectively, for the second motion.

The results of numerical analyses in comparison with experimental results are given in Figures 16–21. The acceleration amplitudes obtained in the numerical models were consistent with the experimental measurements.

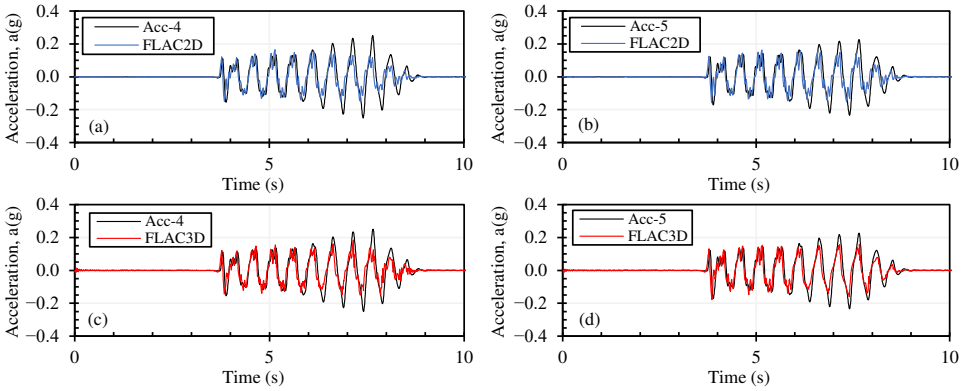

Figure 16. Acc. time histories for the first motion at PPT-1 and PPT-2 elevations: (**a**,**b**) FLAC2D results and (**c**,**d**) FLAC3D results.

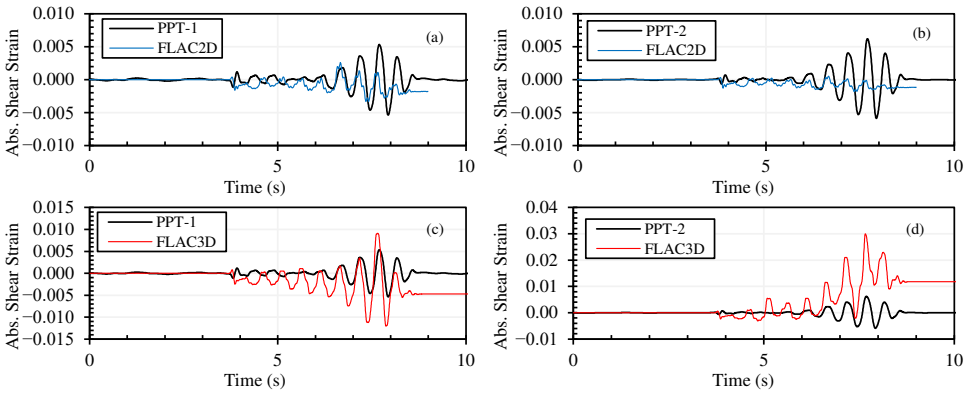

Figure 17. Absolute shear strain time histories for the first motion at PPT-1 and PPT-2 elevations: (**a**,**b**) FLAC2D results and (**c**,**d**) FLAC3D results.

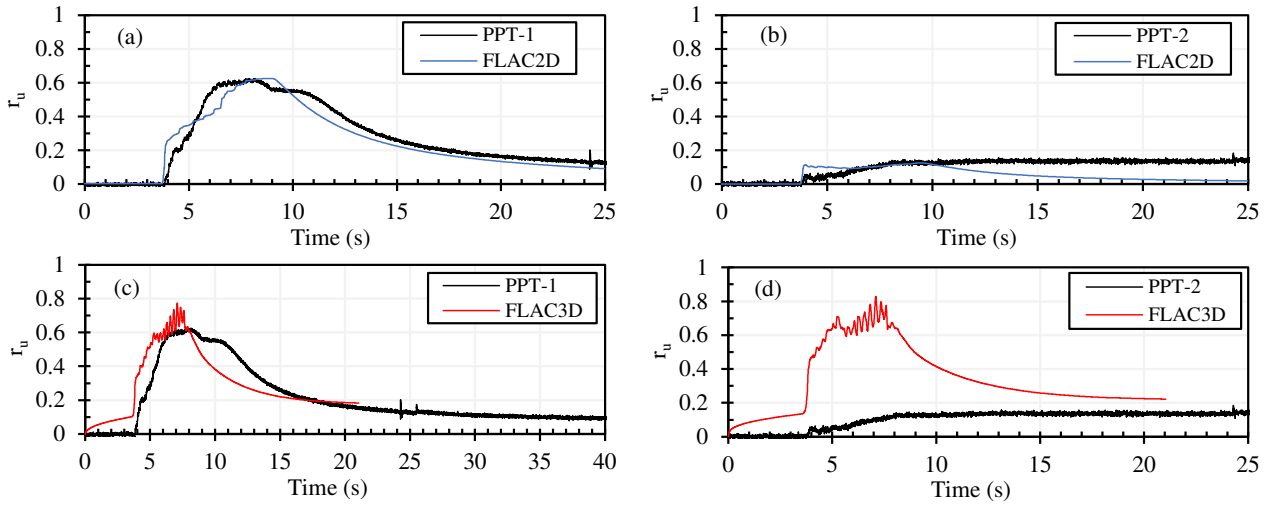

Figure 18. Comparisons of r_u time histories for first motion at PPT-1 and PPT-2 elevations: (**a**,**b**) FLAC2D results and (**c**,**d**) FLAC3D results.

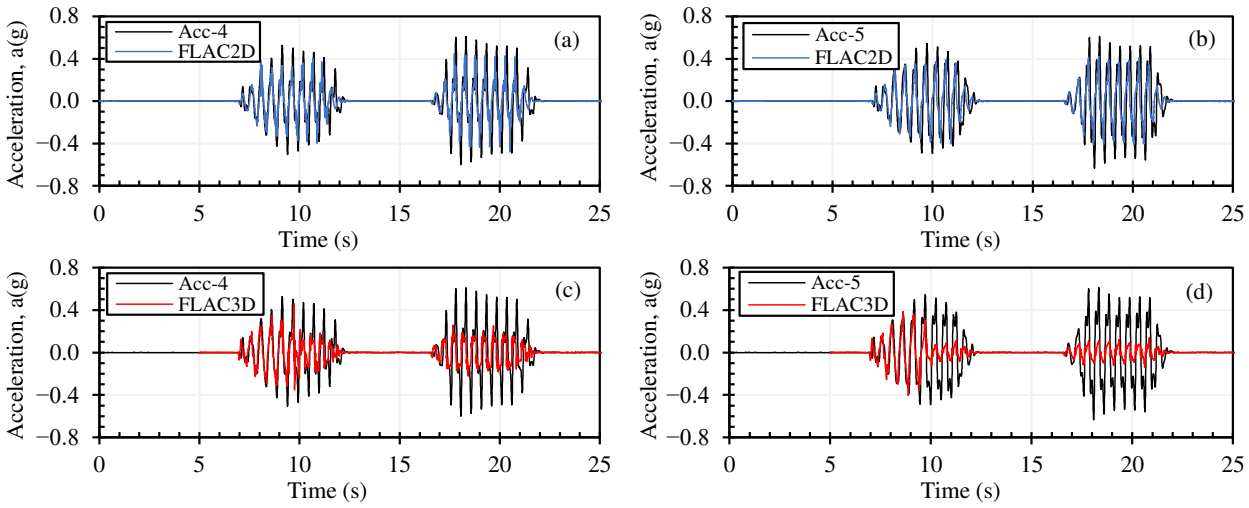

Figure 19. Acc. time histories for the second motion at PPT-1 and PPT-2 elevations: (**a**,**b**) FLAC2D results and (**c**,**d**) FLAC3D results.

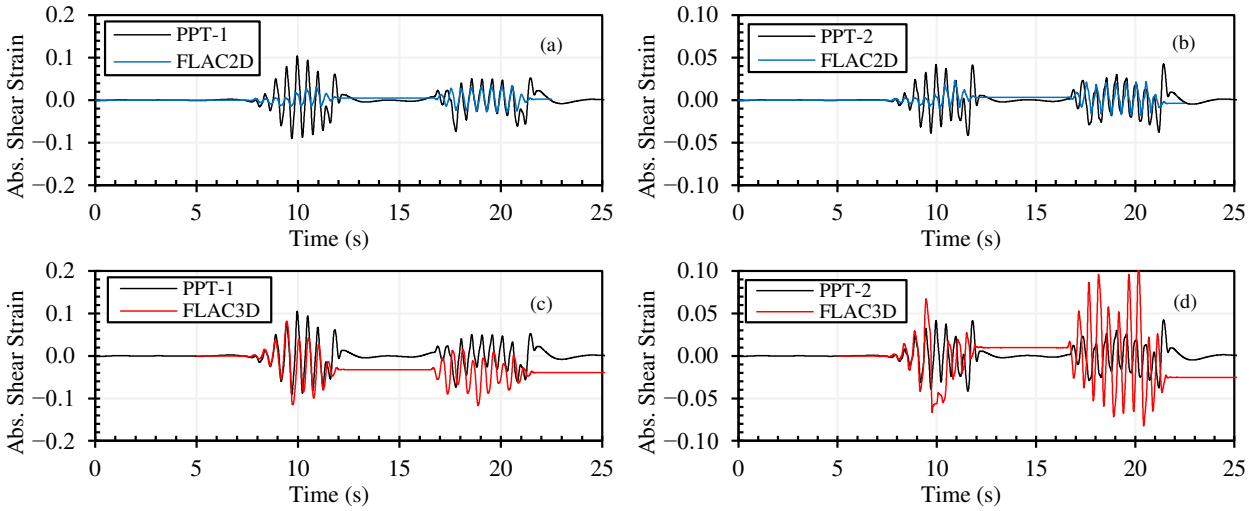

Figure 20. Absolute shear strain time histories for the second motion at PPT-1 and PPT-2 elevations: (**a**,**b**) FLAC2D results and (**c**,**d**) FLAC3D results.

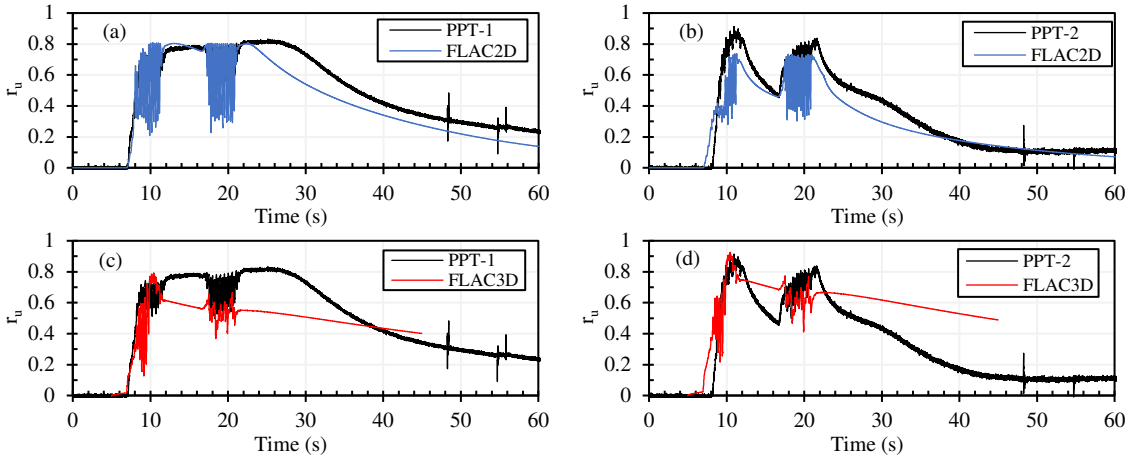

Figure 21. Comparisons of r_u time histories for the second motion at PPT-1 and PPT-2 elevations: (**a**,**b**) FLAC2D results and (**c**,**d**) FLAC3D results.

During the first five loading cycles, the acceleration amplitudes obtained from both the experimental measurements and the numerical simulations were highly consistent at approximately 0.2 g. Following this stage, the experimentally measured acceleration amplitudes increased to about 0.23 g, whereas the numerical results maintained a nearly constant value of 0.2 g (Figure 16). The increase in the experimental amplitudes may be attributed to the effect of hydrodynamics on the accelerations and the rebounding effect of the laminar walls and Sikaflex. The absolute shear strain values calculated at the PPT-1 and PPT-2 levels were compared with the numerical analysis results. While a good agreement is generally observed at the PPT-1 level, the FLAC3D model predicted higher strain amplitudes, particularly at the PPT-2 level (Figure 17). The excess pore water pressure ratio at the PPT-1 elevation gradually rose to approximately 0.6 and subsequently dissipated to around 0.1 within 15 s (Figure 18). This trend, including both the buildup and the rapid dissipation behavior, was successfully captured in the 2D and 3D numerical analyses. At the PPT-2 location, excess pore water pressures were not generated in the experiments, and the 2D numerical model similarly predicted very low pore-pressure development. In contrast, the 3D numerical model significantly overpredicted the excess pore water pressures at this elevation. This discrepancy may be attributed to constitutive model parameters, particularly the plastic modulus parameter determined based on the direct simple shear tests, which may be underestimated and could induce higher shear strains, leading to greater excess pore water pressures (Figure 18).

Figures 19–21 compares the acceleration, absolute shear strains, and pore-pressure responses from the 2D and 3D numerical analyses with the experimental records. The 2D model reproduces the acceleration amplitudes and waveform more closely than the 3D model, which shows noticeable deviations during strong shaking, most probably due to an increase in damping in the P2PSand model after liquefaction triggering. A comparison was made between the absolute shear strain values at the PPT-1 and PPT-2 levels and the results obtained from numerical analyses. A generally good agreement is observed at both levels for both analyses, particularly in terms of the overall response pattern. However, the FLAC3D model predicts higher strain amplitudes, especially at the PPT-2 level, whereas the FLAC2D results remain relatively closer to the experimental values (Figure 20). At PPT-1 and PPT-2, both the 2D and 3D models capture pore-pressure buildup, with a better representation of dissipation in the 2D model compared to the experimental response (Figure 21). Consequently, regarding the r_u trend, despite slight differences in the magnitudes of soil acceleration and r_u values, numerical analysis results show that the

calibrated model parameters accurately represent the dynamic response of the soil inside the laminar box.

Based on the comparison between the experimental results and the numerical simulations, the 2D model provides a decent representation of the shaking table response in the newly developed ETILam soil container. The 2D analysis reasonably reproduces both the acceleration time histories and the pore-pressure-generation patterns at the monitored elevations. Given this consistent agreement, the 2D numerical model can be preferred for future soil–structure interaction studies involving the same container configuration and soil conditions, rather than a 3D model that may require excessive time and data storage. Additionally, the influence of the flow-on and flow-off options was examined to support future modeling studies.

The impact of flow over the entire time history was analyzed through two-dimensional numerical simulations, both with and without considering flow, and the results are presented in Figures 22 and 23. In both motions, the flow-on option resulted in a smoother transition from the shaking phase to the post-liquefaction reconsolidation stage. Additionally, for the second motion, the flow-on option more accurately captured the dissipation behavior observed between the two consecutive shakings.

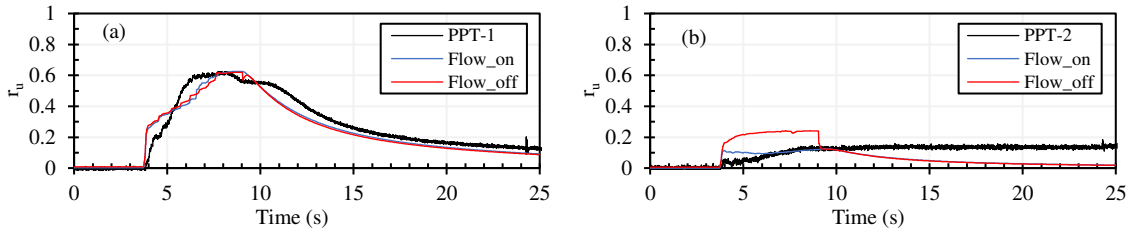

Figure 22. Flow effect on the r_u time histories for the first motion at PPT-1 and PPT-2 elevations: (**a**) PPT-1 and (**b**) PPT-2.

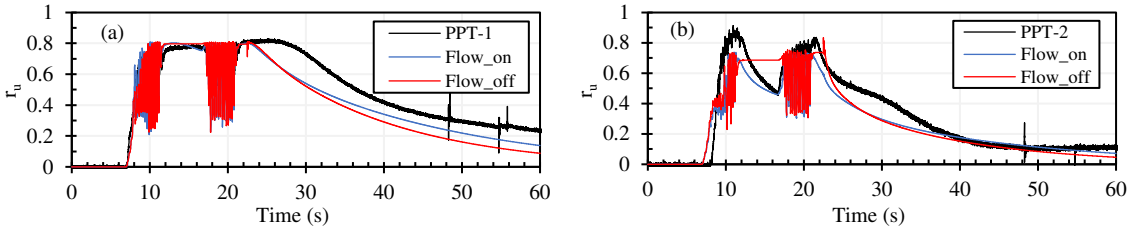

Figure 23. Flow effect on the r_u time histories at the second motion at PPT-1 and PPT-2 elevations: (**a**) PPT-1 and (**b**) PPT-2.

4. Summary and Conclusions

A comprehensive experimental and numerical study was conducted to investigate the liquefaction behavior of saturated sands using the newly proposed and patented ETILam (Enhanced Transparent Impermeable Laminar) soil container. The container, designed to better simulate free-field 1D soil response while allowing accurate instrumentation, impermeability, and observation, was used to prepare a sand specimen consisting of dense and loose saturated sand layers topped by dry sand. The performance of ETILam in testing the liquefaction behavior of sands was evaluated. The specimen preparation procedures, especially those developed for ETILam, and the instrument alignment were presented in detail. Two harmonic input motions (0.1 g–2 Hz and 0.2 g–2 Hz), the second motion being two consecutive 6 s excitations, were applied on a uniaxial shaking table. The system's dynamic behavior was evaluated through acceleration time histories, shear-strains, excess pore water pressure measurements, response spectra, and Fourier amplitude computations.

Fully coupled effective-stress analyses were performed to numerically model these experiments using the PM4Sand and P2PSand constitutive models in 2D and 3D, respectively, within the FLAC2D 8.1 and FLAC3D 7.0 software programs. Calibration studies were carried out considering CDSS experiments performed at different cyclic stress ratio (CSR) values. These calibration studies were performed on Sile Sand samples prepared at three relative densities to determine the input parameters for the PM4Sand (for 2D analyses) and P2PSand (for 3D analyses) constitutive models. Following calibration, 2D and 3D numerical models were developed to simulate soil behavior in the laminar box by providing similar boundary conditions, and tested under two different shaking motions.

Liquefaction triggering and reconsolidation trends were clearly observed. Particularly, the r_u did not reach 0.8–1.0 at 0.5%, which reveals that liquefaction did not occur completely, whereas in the second motion, shear strains reached 10%, and r_u approached 0.8, confirming liquefaction triggering. During the subsequent 6 s motions, excess pore water pressures at deeper levels were not dissipated and remained at the maximum value, while at the levels closer to the surface, r_u started to dissipate during the non-shaking period and then regenerated rapidly once the latter 6 s motion started.

Comparisons of our experiments with the numerical models demonstrated that acceleration amplitudes were reproduced well by both the 2D and 3D models. The 2D model demonstrated strong agreement with experimental results, accurately reproducing acceleration amplitudes, pore-pressure-generation patterns, dissipation behavior, and depth-dependent response. Pore-pressure generation at a deeper level was captured by both models; however, the 3D model overpredicted pore pressure at a closer level to the surface, whereas the 2D model aligned more closely with experimental behavior. The dissipation patterns between sequential motions were also better represented in the 2D analyses.

Additional analyses, where flow-on versus flow-off options were examined, indicated that enabling flow resulted in a more realistic transition from shaking to post-liquefaction reconsolidation, particularly for the second motion, where partial dissipation occurred between consecutive shaking phases. Overall, the combined experimental and numerical findings validate both the ETILam container design and the sufficiency of a well-calibrated 2D numerical approach for studying liquefaction within this system.

For future publications, soil–structure interaction (SSI) experiments conducted in liquifiable sands in ETILam will be reported and compared with the numerical models calibrated and verified in this study.

Supplementary Materials: The following supporting information can be downloaded at: https://www.mdpi.com/article/10.3390/app16094572/s1, Video S1: 0.1g_Free_Field.mp4, Video S2: 0.2g_Free_Field.mp4.

Author Contributions: Conceptualization, methodology: E.E.E.-B. and M.B.K.; experimental work: B.K., M.B.K., E.G. and E.E.E.-B.; data processing: M.B.K., E.G., B.K. and E.E.E.-B.; numerical analyses: M.B.K. and O.A.; writing—original draft preparation: M.B.K. and O.A.; project administration, supervision, funding acquisition, paper writing, editing: E.E.E.-B. All authors have read and agreed to the published version of the manuscript.

Funding: This research was funded by TUBITAK (The Scientific and Technological Research Council of Turkiye) under Grant No. 121M757 and project title "Development of the Design Criteria for Buildings in Liquefiable Soils with Emphasize on Foundation Type and Soil-Structure Interaction" and by the BAP (Scientific Research Projects) Department of Istanbul Technical University, under the Project Number: MGA-2024-45712 and project title "Determination of the Effects of Soil–Structure Interaction on Pore Water Pressure and Foundation Accelerations in Clayey and Sandy Soils under Seismic Loads through Large-Scale Experiments".

Institutional Review Board Statement: Not applicable, as this study does not involve human or animal subjects.

Informed Consent Statement: Not applicable.

Data Availability Statement: The dataset generated during and/or analyzed during the current study is available from the authors on reasonable request.

Acknowledgments: The support of TUBITAK under the 1001 Project with number 121M757 and BAP under MGA-2024-45712 Project was greatly appreciated. The authors appreciate the invaluable support of the Structural and Earthquake Laboratory Coordinator, Ercan Yüksel; the Vice coordinators, Yavuz Durgun, Hakan Saruhan, and Fatih Şahin; the technicians, Mahmut Şamli and Turgay Özgünay; and the undergraduate student Ali Bahçeci.

Conflicts of Interest: The authors declare no conflicts of interest.

References

1. Dashti, S.; Bray, J.D.; Pestana, J.M.; Riemer, M.; Wilson, D. Centrifuge testing to evaluate and mitigate liquefaction-induced building settlement mechanisms. *J. Geotech. Geoenviron. Eng.* **2010**, *136*, 918–929. [CrossRef]
2. Karimi, Z.; Dashti, S. Numerical and centrifuge modeling of seismic soil–foundation–structure interaction on liquefiable ground. *J. Geotech. Geoenviron. Eng.* **2016**, *142*, 04015061. [CrossRef]
3. Jafarian, Y.; Mehrzad, B.; Lee, C.J.; Haddad, A.H. Centrifuge modeling of seismic foundation-soil-foundation interaction on liquefiable sand. *Soil Dyn. Earthq. Eng.* **2017**, *97*, 184–204. [CrossRef]
4. Olarte, J.; Paramasivam, B.; Dashti, S.; Liel, A.; Zannin, J. Centrifuge modeling of mitigation-soil-foundation-structure interaction on liquefiable ground. *Soil Dyn. Earthq. Eng.* **2017**, *97*, 304–323. [CrossRef]
5. Ramirez, J.; Barrero, A.R.; Chen, L.; Dashti, S.; Ghofrani, A.; Taiebat, M.; Arduino, P. Site response in a layered liquefiable deposit: Evaluation of different numerical tools and methodologies with centrifuge experimental results. *J. Geotech. Geoenviron. Eng.* **2018**, *144*, 04018073. [CrossRef]
6. Adamidis, O.; Madabhushi, S.P.G. Experimental investigation of drainage during earthquake-induced liquefaction. *Géotechnique* **2018**, *68*, 655–665. [CrossRef]
7. Mehrzad, B.; Jafarian, Y.; Lee, C.J.; Haddad, A.H. Centrifuge study into the effect of liquefaction extent on permanent settlement and seismic response of shallow foundations. *Soils Found.* **2018**, *58*, 228–240. [CrossRef]
8. Ye, B.; Zhang, L.; Wang, H.; Zhang, X.; Lu, P.; Ren, F. Centrifuge model testing on reliquefaction characteristics of sand. *Bull. Earthq. Eng.* **2019**, *17*, 141–157. [CrossRef]
9. Bouckovalas, G.D.; Tsiapas, Y.Z.; Theocharis, A.I.; Chaloulos, Y.K. Ground response at liquefied sites: Seismic isolation or amplification? *Soil Dyn. Earthq. Eng.* **2016**, *91*, 329–339. [CrossRef]
10. Adampira, M.; Derakhshandi, M. Influence of a layered liquefiable soil on seismic site response using physical modeling and numerical simulation. *Eng. Geol.* **2020**, *266*, 105462. [CrossRef]
11. Adampira, M.; Derakhshandi, M.; Ghalandarzadeh, A. Experimental study on seismic response characteristics of liquefiable soil layers. *J. Earthq. Eng.* **2021**, *25*, 1287–1315. [CrossRef]
12. Ko, Y.Y.; Chen, C.H. On the variation of mechanical properties of saturated sand during liquefaction observed in shaking table tests. *Soil Dyn. Earthq. Eng.* **2020**, *129*, 105946. [CrossRef]
13. Basu, D.; Montgomery, J.; Stuedlein, A.W. Observations and challenges in simulating post-liquefaction settlements from centrifuge and shake table tests. *Soil Dyn. Earthq. Eng.* **2022**, *153*, 107089. [CrossRef]
14. Toyota, H.; Towhata, I.; Imamura, S.I.; Kudo, K.I. Shaking table tests on flow dynamics in liquefied slope. *Soils Found.* **2004**, *44*, 67–84. [CrossRef] [PubMed]
15. Wang, J.; Salam, S.; Xiao, M. Evaluation of the effects of shaking history on liquefaction and cone penetration resistance using shake table tests. *Soil Dyn. Earthq. Eng.* **2020**, *131*, 106025. [CrossRef]
16. Yao, C.; Zhong, H.; Zhu, Z. Development of a large shaking table test for sand liquefaction analysis. *Lithosphere* **2024**, *2024*, lithosphere_2024_137. [CrossRef]
17. Ecemis, N. Experimental and numerical modeling on the liquefaction potential and ground settlement of silt-interlayered stratified sands. *Soil Dyn. Earthq. Eng.* **2021**, *144*, 106691. [CrossRef]
18. Dou, P.; Xu, C.; Du, X.; Chen, S. Influence of structure on the aseismic stability and dynamic responses of liquefiable soil. *Bull. Earthq. Eng.* **2022**, *20*, 55–76. [CrossRef]
19. Mittal, V.; Samanta, M. Performance of a Laminar Shear Box for Cohesionless Soil Under Seismic Excitations. *Geotech. Geol. Eng.* **2025**, *43*, 60. [CrossRef]

20. Mohsan, M.; Kiyota, T.; Umar, M.; Katagiri, T. Effect of Pavement Thickness and Width on Liquefaction-Induced Settlements and the Contribution of Sand Ejecta in Total Settlement. *Geotech. Geol. Eng.* **2021**, *39*, 4523–4531. [CrossRef]
21. Li, X.; Pan, D.; Huang, Y.; Cheng, Y.; Fu, X. Shaking table test and numerical simulation of free field in sand-sawdust mixed soil. *Soil Dyn. Earthq. Eng.* **2023**, *165*, 107707. [CrossRef]
22. Fan, Z.; Yuan, Y.; Cudmani, R.; Deng, J.; Chrisopoulos, S.; Vogt, S.; Niebler, M. Large biaxial laminar shear box for 1-g shaking table tests on saturated sand. *Soil Dyn. Earthq. Eng.* **2024**, *183*, 108756. [CrossRef]
23. Bagheri, O.; Eseller-Bayat, E.E. Laminar Soil Container's Performance Study for Dynamic Laboratory Tests: Comprehensive Review and Numerical Verification. *KSCE J. Civ. Eng.* **2024**, *28*, 2705–2721. [CrossRef]
24. Bagheri, O.; Gündüz, M.Ş.; Alver, O.; Eseller-Bayat, E.E. A New Design for Large-Scale Dynamic Soil Testing Setup: ETILam (Enhanced Transparent Impermeable Laminar) Soil Container. *J. Earthq. Eng.* **2026**, 1–23. [CrossRef]
25. TDG Ankara-Türkiye. Available online: https://tdg.com.tr/en/products/earthquake-simulators/servo-hydraulic/tdg-high-capacity-shake-table (accessed on 24 March 2026).
26. TDG Ankara-Türkiye. Available online: https://tdg.com.tr/tr/urunler/ivmeolcer---tiltmetre---sensorler/tiltmetreler/sensebox7001-t (accessed on 15 January 2026).
27. ACE, South Korea. Available online: http://aceco.co.kr/home_en/pro_08.php (accessed on 18 January 2026).
28. TML, Japan. Available online: https://tml.jp/e/product/transducers/displacement_high.html (accessed on 16 January 2026).
29. Gurbanov, E. Test Procedure and Sample Preparation for Large Scale Soil Structure Interaction Model Tests in Eitlsc. Master's Thesis, Istanbul Technical University, Istanbul, Türkiye, 2024.
30. Tsuchida, H. Prediction and countermeasure against the liquefaction in sand deposits. In *Abstract of the Seminar in the Port and Harbor Research Institute*; Ministry of Transport: Yokosuka, Japan, 1970; pp. 31–333.
31. Itasca Consulting Group, Inc. *FLAC—Fast Lagrangian Analysis of Continua, Ver. 8.1*; Itasca: Minneapolis, MN, USA, 2019.
32. Itasca Consulting Group, Inc. *FLAC3D—Fast Lagrangian Analysis of Continua in Three-Dimensions, Ver. 7.0*; Itasca: Minneapolis, MN, USA, 2019.
33. Ziotopoulou, K.; Boulanger, R.W. Plasticity modeling of liquefaction effects under sloping ground and irregular cyclic loading conditions. *Soil Dyn. Earthq. Eng.* **2016**, *84*, 269–283. [CrossRef]
34. Dafalias, Y.F.; Manzari, M.T. Simple plasticity sand model accounting for fabric change effects. *J. Eng. Mech.* **2004**, *130*, 622–634. [CrossRef]
35. Cheng, Z.; Detournay, C. Formulation, validation and application of a practice-oriented two-surface plasticity sand model. *Comput. Geotech.* **2021**, *132*, 103984. [CrossRef]
36. Deniz, O. Development of Liquefaction Resistance Curves of Partially Saturated Sands. Master's Thesis, Istanbul Technical University, Istanbul, Türkiye, 2021.
37. Boulanger, R.W.; Idriss, I.M. CPT-based liquefaction triggering procedure. *J. Geotech. Geoenviron. Eng.* **2016**, *142*, 04015065. [CrossRef]